NASA / CR-2002-211753

Development of an Efficient Binaural Simulation for the Analysis of Structural Acoustic Data

Aimee L. Lalime and Marty E. Johnson
Virginia Polytechnic Institute and State University
Blacksburg, Virginia

July 2002

The NASA STI Program Office ... in Profile

Since its founding, NASA has been dedicated to the advancement of aeronautics and space science. The NASA Scientific and Technical Information (STI) Program Office plays a key part in helping NASA maintain this important role.

The NASA STI Program Office is operated by Langley Research Center, the lead center for NASA's scientific and technical information. The NASA STI Program Office provides access to the NASA STI Database, the largest collection of aeronautical and space science STI in the world. The Program Office is also NASA's institutional mechanism for disseminating the results of its research and development activities. These results are published by NASA in the NASA STI Report Series, which includes the following report types:

- TECHNICAL PUBLICATION. Reports of completed research or a major significant phase of research that present the results of NASA programs and include extensive data or theoretical analysis. Includes compilations of significant scientific and technical data and information deemed to be of continuing reference value. NASA counterpart of peer-reviewed formal professional papers, but having less stringent limitations on manuscript length and extent of graphic presentations.

- TECHNICAL MEMORANDUM. Scientific and technical findings that are preliminary or of specialized interest, e.g., quick release reports, working papers, and bibliographies that contain minimal annotation. Does not contain extensive analysis.

- CONTRACTOR REPORT. Scientific and technical findings by NASA-sponsored contractors and grantees.

- CONFERENCE PUBLICATION. Collected papers from scientific and technical conferences, symposia, seminars, or other meetings sponsored or co-sponsored by NASA.

- SPECIAL PUBLICATION. Scientific, technical, or historical information from NASA programs, projects, and missions, often concerned with subjects having substantial public interest.

- TECHNICAL TRANSLATION. English-language translations of foreign scientific and technical material pertinent to NASA's mission.

Specialized services that complement the STI Program Office's diverse offerings include creating custom thesauri, building customized databases, organizing and publishing research results ... even providing videos.

For more information about the NASA STI Program Office, see the following:

- Access the NASA STI Program Home Page at ***http://www.sti.nasa.gov***

- E-mail your question via the Internet to help@sti.nasa.gov

- Fax your question to the NASA STI Help Desk at (301) 621-0134

- Phone the NASA STI Help Desk at (301) 621-0390

- Write to:
  NASA STI Help Desk
  NASA Center for AeroSpace Information
  7121 Standard Drive
  Hanover, MD 21076-1320

NASA / CR-2002-211753

Development of an Efficient Binaural Simulation for the Analysis of Structural Acoustic Data

Aimee L. Lalime and Marty E. Johnson
Virginia Polytechnic Institute and State University
Blacksburg, Virginia

National Aeronautics and
Space Administration

Langley Research Center
Hampton, Virginia 23681-2199

Prepared for Langley Research Center
under Cooperative Agreement NCC1-01029

July 2002

The use of trademarks or names of manufacturers in the report is for accurate reporting and does not constitute an official endorsement, either expressed or implied, of such products or manufacturers by the National Aeronautics and Space Administration.

Available from:

NASA Center for AeroSpace Information (CASI)
7121 Standard Drive
Hanover, MD 21076-1320
(301) 621-0390

National Technical Information Service (NTIS)
5285 Port Royal Road
Springfield, VA 22161-2171
(703) 605-6000

Foreword

This report summarizes the research accomplishments performed under the NASA Langley Research Center research cooperative agreement no. NCC1-01029 entitled, "Development of an Efficient Binaural Simulation for the Analysis of Structural Acoustic Data." Funding for the work was provided by the Life Cycle Simulation element of the NASA Intelligent Synthesis Environment Program under the task entitled "Structural Acoustic Simulation in Operational Environments." Dr. Stephen A. Rizzi of the NASA Langley Research Center was the ISE task lead and technical officer of this cooperative agreement.

Contents

Abstract

Binaural or “virtual acoustic” representation has been proposed as a method of analyzing acoustic and vibro-acoustic data. Unfortunately, this binaural representation can require extensive computer power to apply the Head Related Transfer Functions (HRTFs) to a large number of sources, as with a vibrating structure. This work focuses on reducing the number of real-time computations required in this binaural analysis through the use of Singular Value Decomposition (SVD) and Equivalent Source Reduction (ESR). The SVD method reduces the complexity of the HRTF computations by breaking the HRTFs into dominant singular values (and vectors). The ESR method reduces the number of sources to be analyzed in real-time computation by replacing sources on the scale of a structural wavelength with sources on the scale of an acoustic wavelength. It is shown that the effectiveness of the SVD and ESR methods improves as the complexity of the source increases. In addition, preliminary auralization tests have shown that the results from both the SVD and ESR methods are indistinguishable from the results found with the exhaustive method.

Introduction

Improvements in digital acquisition and sensor technology have led to an increase in the ability to acquire large data sets. One potential way of analyzing structural acoustic data is the creation of a three-dimensional audio-visual environment. For example, an audio-visual virtual representation of the inside of the space station could allow designers and astronauts to experience and analyze the acoustic properties of the space station. Incorporating the visual aspect with the acoustic allows the user to sift rapidly through noise data to determine what parts of a vibrating structure are radiating sound to what areas in an acoustic enclosure.

Unfortunately, the three-dimensional (or binaural) simulation of structural data is not currently feasible because of the large number of computations required to analyze a distributed source. The objective of this research has been to reduce the number of calculations required to calculate the binaural signals of an acoustically large source. Both pre-processing and real-time reduction methods will be discussed.

Binaural literally means “two ears”, and is a term used to describe three-dimensional sound [1]. Humans detect the direction of sound using the differences in the sound that is heard by each ear. For example, a sound from the right will be louder in the right ear than in the left. This sound level difference is termed Interaural Intensity Difference (IID) and is one of the most important aural cues for localizing sound. Another localization cue is the Interaural Time Difference, or ITD [2]. This is the difference in the amount of time taken for a sound to reach each ear. In the preceding example, the sound coming from the right of the head is heard by the right ear less than 1ms before being sensed by the left ear. This small ITD is sensed by the brain and used to determine the location of the sound source.

IID and ITD are mathematically described in the transfer function between a sound source and the left and right ears, termed the Head Related Transfer Function (HRTF). HRTFs describe not only IID and ITD, but also how sound is affected by its interaction with the head, torso, and ear. For example, as sound approaches the head, low frequency sound wraps around the head, reaching both ears. However, with high frequencies a shadowing effect occurs, causing the high frequency content to be sensed on one side of the head and not the other. Sound also reflects off the subject's torso, causing time and intensity changes. The outer ear also affects the sound entering the ear, as its shape causes the sound to resonate at certain frequencies. Head Related Transfer Functions can be used to calculate the binaural signals at a listener's ears, thereby simulating a three-dimensional sound field around a subject's head. [1]

Unfortunately, the application of the HRTFs is computationally expensive, and restricts real-time binaural analysis of a large number of sources (as with a vibrating structure). A great deal of research has been done on the modeling of HRTFs including Principal Components Analysis [3, 4], Karhunen-Loeve Expansion [5, 6], Balanced Model Truncation [7], State-Space Analysis [8, 9], Representation as Spherical Harmonics [10, 11], Pole-Zero Approximation [12, 13], and Structural Modeling [14, 15]. Duda [16] presents a comprehensive summary of these different HRTF models, which have been researched for several reasons: to better understand the properties of HRTFs, to reduce the number of measurements required in order to create a full set of individualized HRTFs, and (as with this research) to reduce the number and complexity of real-time calculations. This research uses Singular Value Decomposition (SVD) to model the HRTFs, which is based on series expansion, as are Principal Components Analysis and Karhunen-Loeve Expansion.

This research also uses the Equivalent Source Reduction (ESR) [17] in order to simplify the binaural simulation of a distributed source. This research combines the ESR and SVD methods and applies them to the binaural simulation of structural acoustic data, which is a new research area in binaural acoustics.

The theory behind the binaural simulation of acoustic data is discussed in the first section of this report. From there, the current technology for calculating the binaural signals is examined in the "Exhaustive Method" portion of the report. Also included in the Exhaustive Method section is a description of how each step of the exhaustive method was verified by comparing the results with actual test data. The next section, termed "Reduction Methods", details the investigation of the proposed methods for reducing the computation time of the exhaustive method. Included in the Reduction Methods section are the discussions of SVD, ESR, and the estimated reduction in computation time resulting from the use of SVD and ESR. Lastly, conclusions are drawn regarding the effectiveness and potential use of the reduction methods in real-time structural acoustic analysis.

Theory

In order to discuss the exhaustive and reduced methods of simulating the binaural signals associated with structural acoustics, there are several topics that must be understood and discussed. The first is a discussion on how sound radiates from a monopole source. Following will be descriptions involving HRTF's use in binaural simulation, including: the binaural simulation of sound radiating from a monopole; how the implementation of HRTFs changes with sampled signals rather than analog ones; the binaural simulation of multiple sources; and the binaural simulation of a vibrating plate.

Radiation from a Monopole

The simplest acoustic source is that of a pulsating sphere, also known as a monopole (figure 1). According to Fahy's, *Engineering Acoustics*, the sound pressure at a radial distance, *r*, caused by the radiation from a monopole source is defined according to equation 1 [18]:

$$p(r,t) = \left(\frac{\rho_0}{4\pi r}\right)\frac{\partial}{\partial t}\left[Q\left(t-\frac{r}{c}\right)\right] \tag{1}$$

where ρ_o is the density of air and Q is the volume velocity. Q is defined according to equation 2 [19]:

$$Q = Su \tag{2}$$

where S is the surface area of the sphere ($4\pi r_o^2$) and u is the velocity of the surface of the sphere.

In the case of a vibrating hemisphere rather than a vibrating sphere, the pressure at some distance, *r*, will be

$$p(r,t) = \left(\frac{\rho_0}{2\pi r}\right)\frac{\partial}{\partial t}\left[Q\left(t-\frac{r}{c}\right)\right] \tag{3}$$

$$= \left(\frac{\rho_0 S}{2\pi r}\right)a\left(t-\frac{r}{c}\right) \tag{4}$$

where a is the acceleration of the surface of the pulsating sphere (figure 1). This means that the sound at point R (which is a distance, *r*, from the pulsating sphere) will have a magnitude that varies inversely with the distance, *r*, and a time delay equal to the time it takes for the sound to reach point R, which will be r/c.

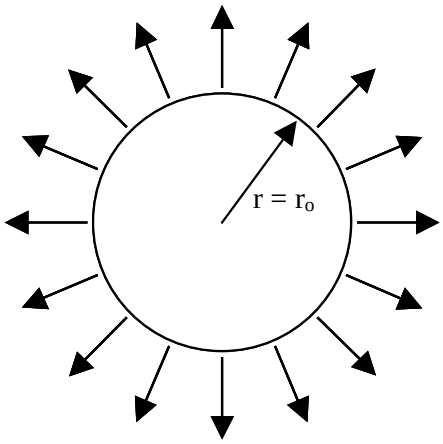

Figure 1: Pulsating Sphere

Head Related Transfer Functions (HRTFs)

As mentioned in the introduction, HRTFs are a set of transfer functions that describe how sound is reflected off the human torso, wraps around the head, and resonates in the inner and outer ear. Because the human body is not axisymmetric, the HRTFs vary depending upon the elevation angle, ϕ, and the circumferential angle, θ, of the sound source. Since every human torso, head, and ears are different, each person has their own individual HRTFs. A generalized set of HRTFs can be obtained using the Knowles Electronic Manikin for Acoustic Research (KEMAR). The KEMAR manikin (figure 2) has a head, torso, and ears that are specifically shaped in order to represent the average human form.

Figure 2: Knowles Electronic Manikin for Acoustic Research

In the time domain, the HRTF represents the impulse response between a source of sound and a human's ears. The convolution integral used to find the sound pressure at the left ear, $p_{L,\theta,\phi}$, due to a monopole source is shown below in equation 5 (figure 3b). The pressure, $p_{\theta,\phi}$, resulting from a monopole at angles θ, ϕ with respect to the head, represents the pressure at the center of the head *if the head were not present* (figure 3a).

$$p_{L,\theta,\phi}(t) = \int_0^t hrtf_{L,\theta,\phi}(\tau)\, p_{\theta,\phi}(t-\tau)\, d\tau \qquad (5)$$

where θ is the circumferential angle between the center of the head and the source,
ϕ is the elevation angle between the center of the head and the source,
$hrtf_L$ is the head related impulse response for the left ear,
and τ is a temporal variable.

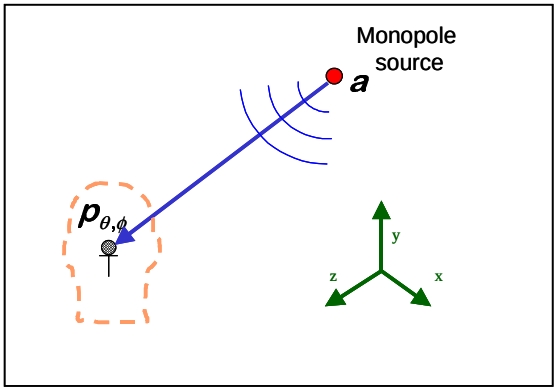

Figure 3a: Pressure at head center

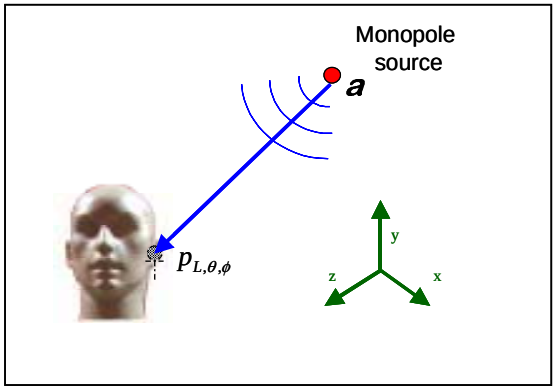

Figure 3b: Pressure at left ear

Note that because the pressure $p_{\theta,\phi}$, is used, the HRTF itself does not contain the 1/r attenuation or the r/c delay. A similar equation can be written to describe the response at the right ear. The angles, θ and ϕ are defined according to figure 4.

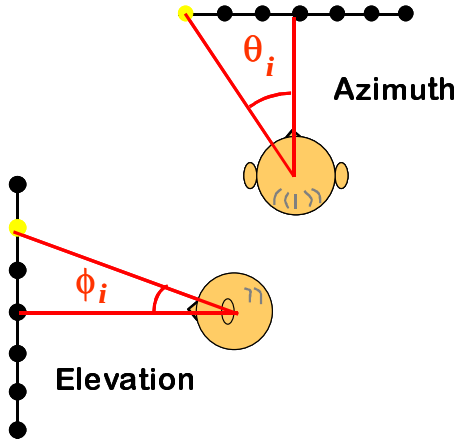

Figure 4: θ and ϕ are measured from the center of the head

Using Sampled Signals

Equation 5 describes the process for finding the sound at the average human's left ear for a *continuous* signal from a monopole source. Since the binaural signals are calculated using a computer, the convolution is actually made up of discrete signals rather than continuous ones. This results in the convolution shown in equation 6.

$$p_{L,\theta,\phi}[i] = \sum_{j=0}^{M-1} hrtf_{L,\theta,\phi}[j]\, p_{\theta,\phi}[i-j] \tag{6}$$

Here M is the number of samples used in the HRTF and i is the i^{th} discrete time step.

In addition, the HRTFs are defined and cataloged only at discrete angles. In this analysis the authors used generalized HRTFs that were recorded at the ears of a KEMAR dummy head (Pinnae type DB-065) by researchers at MIT. These HRTFs can be found at http://web.media.mit.edu/~kdm/hrtf.html [20]. The HRTFs in the MIT set are defined from -40° to 90° with an elevation step of 10°. Since the HRTFs are defined spherically, the degree step in the circumferential direction is different for each elevation. Figure 5 shows the different circumferential angle steps for each elevation. (Note: the circumferential angle steps are in purple and the elevations are in red.) Further note that the MIT HRTFs are not a minimum phase representation, that is, the delay between the right and left ears are contained in the HRTF itself, rather than in a delay look-up table. This has relevance in the preprocessing required in the SVD reduction method.

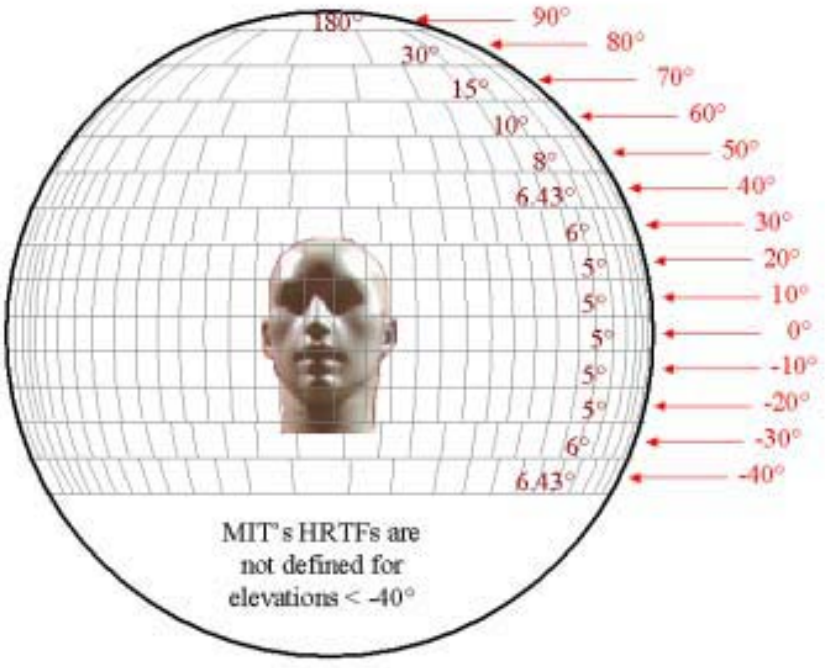

Figure 5: Angles for which MIT's HRTFs are defined and cataloged

Multiple Sources

Having determined how to find the binaural signals resulting from a single source, it is important to find the binaural signals resulting from a group of sources. Equation 6 is linear; therefore, linear superposition can be implemented. Equation 7 shows the total pressure at the left ear resulting from *N* number of sources:

$$p_L[i] = \sum_{n=1}^{N} y_{L,\theta_n,\phi_n}[j] = \sum_{n=1}^{N}\sum_{j=0}^{M-1} hrtf_{L,\theta_n,\phi_n}[j]\, p_{\theta_n,\phi_n}[i-j] \tag{7}$$

An example of this is shown below in figure 6. The pressure at the left ear due to each of three monopole sources is summed to equal p_L. This linear superposition process can be applied to any number of sources.

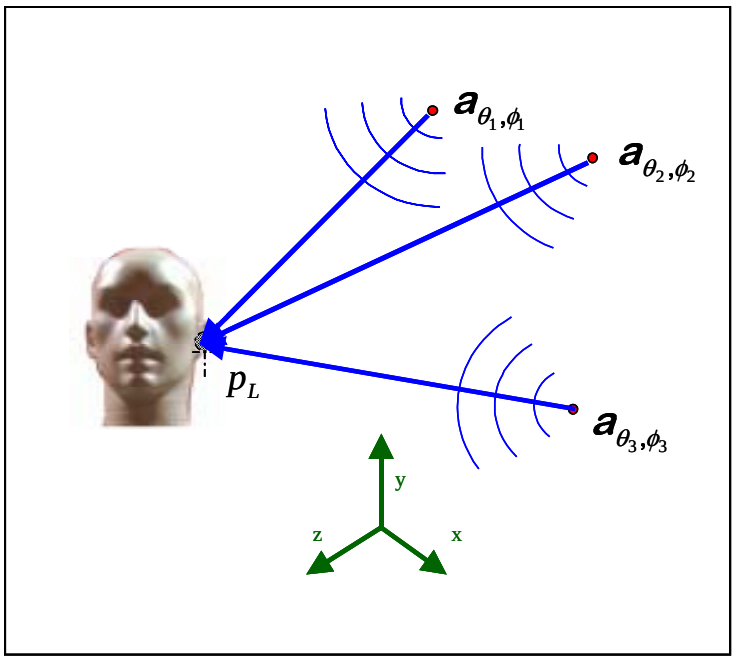

Figure 6: Three monopoles radiating sound to the left ear

Modeling a Vibrating Plate

The goal of this research is find efficient ways to analyze structural acoustic data through binaural simulation. To develop these efficient methods, the authors have chosen to focus on the analysis of a vibrating plate. This plate is set in an infinite baffle and radiates sound into the free field. This structure and configuration was chosen for two reasons: 1) the plate is a relatively simple structure to analyze, allowing the research to focus on the binaural processes rather than structural effects, and 2) a plate in this configuration is essentially the same as a plate secured in a baffle, radiating sound into an anechoic chamber, which can be arranged in a typical acoustic laboratory.

It is a common practice among acousticians to replace a vibrating structure with an array of vibrating monopoles [18,19]. The spacing of the monopoles must be less than half the structural and acoustic wavelengths. Figure 7 shows the sound vibrating from an array of monopole sources, which are used in place of the vibrating plate. This approximation can also be extended to more complex structures should they be considered in future work.

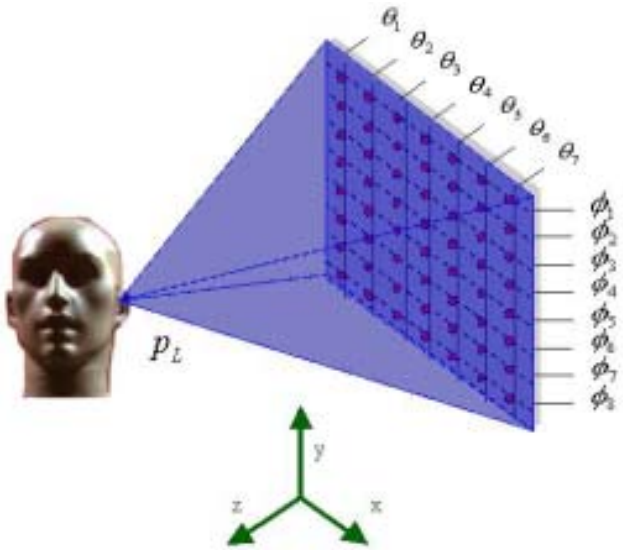

Figure 7: The sound radiated to the left ear by a vibrating plate

Exhaustive Method

The computer process used to calculate the binaural sound radiated from a vibrating structure has been termed the "exhaustive" method because it is based on the current technology and requires a large number of computations. A more detailed description

and a schematic of the exhaustive method will be shown in the first sub-section. Following that will be two sub-sections on verification of two parts of the exhaustive method: the radiation model and the HRTF application. Following will be a discussion of the consistency of the tests that were used to compare with the results of the exhaustive method and a wavenumber decomposition to determine the frequency range for which that data is accurate.

Schematic of the Exhaustive Method

The following is a basic schematic of the exhaustive method (figure 8). The vibrating plate mentioned in the Theory section is modeled as *N* number of monopole sources and the acceleration for each source is defined. The radiation model (equation 4) applies a time delay and gain to the acceleration at each node in order to define the pressure in space caused by each of the vibrating monopoles. Head Related Transfer Functions

(HRTFs) for the left and right ears are then convolved with these pressures (equation 6) to get the pressure at each ear due to each monopole. These pressures are then summed to obtain the same binaural signals as that of someone hearing the sound of a vibrating plate in a free field.

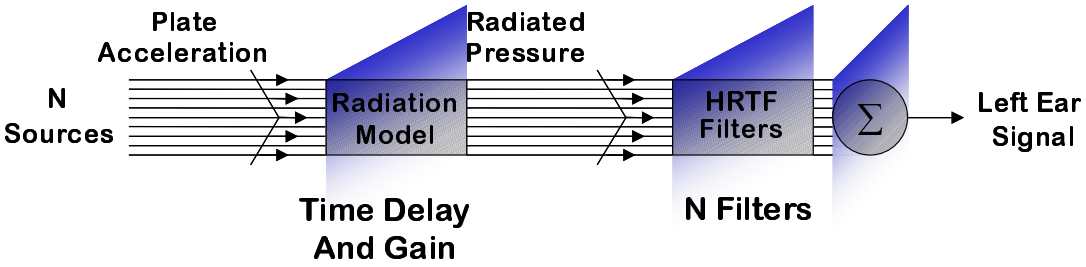

Figure 8: Schematic of the exhaustive method

Verifying Radiation Model

It is important to note that the acceleration of each monopole source can be measured in a laboratory by placing an accelerometer in the same position as the replacement monopole source. This and other data was collected at NASA Langley by Grosveld [21] from a 1.415m x 1.415m x 4.9mm aluminum panel (subjected to mechanical excitation) that was mounted in a transmission-loss facility. Also included in the data set are the transfer functions: from the input force to a microphone in the anechoic chamber, and from the input force to two microphones in the left and right ears of NASA's KEMAR dummy head. The measured plate accelerations were used as input into the exhaustive code (figure 8), the radiated pressure was compared to the microphone transfer function, and the output was compared with the binaural recordings. In this way, each step of the exhaustive method was verified.

The velocity of the plate at each of the 529 nodes was the first set of measurements to be taken. This data was collected using a laser scanning vibrometer (figure 9) and was saved as a transfer function between the input force and the velocity of each node on the plate. This data was collected for two different force positions on the plate.

Figure 9: Laser scanning vibrometer

The following plot (figure 10) is the sum of the squares of the plate velocities, assuming a white noise force input. Notice that the frequency response has very sharp resonance peaks. This is because the test plate was very lightly damped. In fact, this plot actually underestimates the damping because exponential windowing was added to the vibrometer measurements [21].

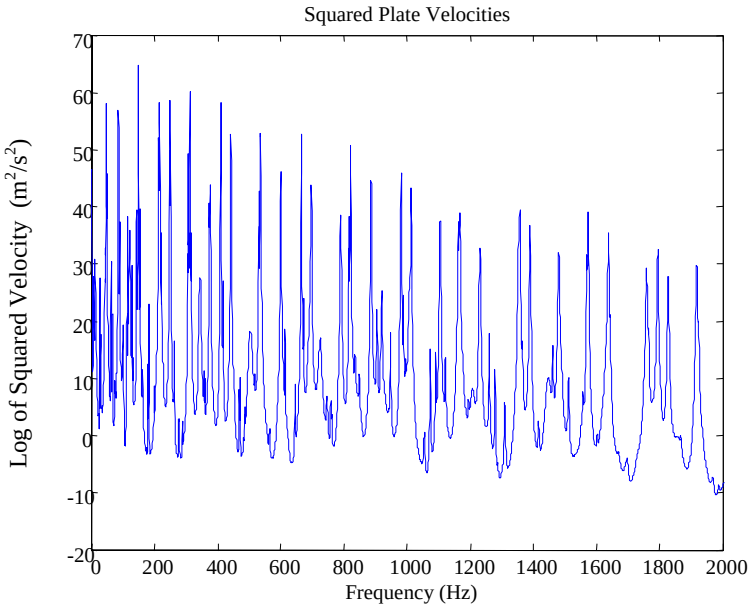

Figure 10: Sum of the squares of the plate velocities

The low damping level of the test plate is also seen in the transfer function (figure 11b) from the input force to a microphone at the position shown in figure 11a.

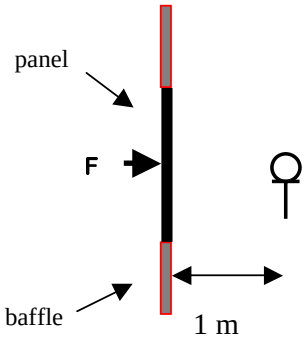

Figure 11a: Microphone configuration in relation to plate

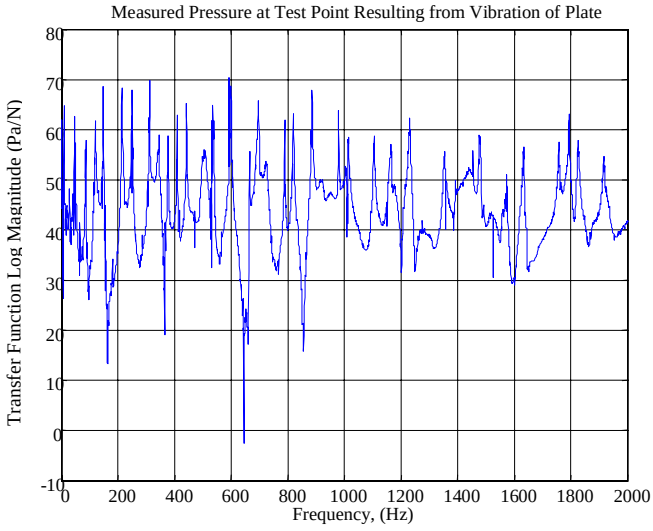

Figure 11b: Measured transfer function at test point

This allows a direct comparison (figure 12) between the calculated and measured transfer functions from the input force to a microphone (as in figure 11a). The calculated pressure was found through the exhaustive method—with *measured* plate velocities used as the input. This calculation was performed in the frequency domain, but is equivalent to the equations presented in the Theory section.

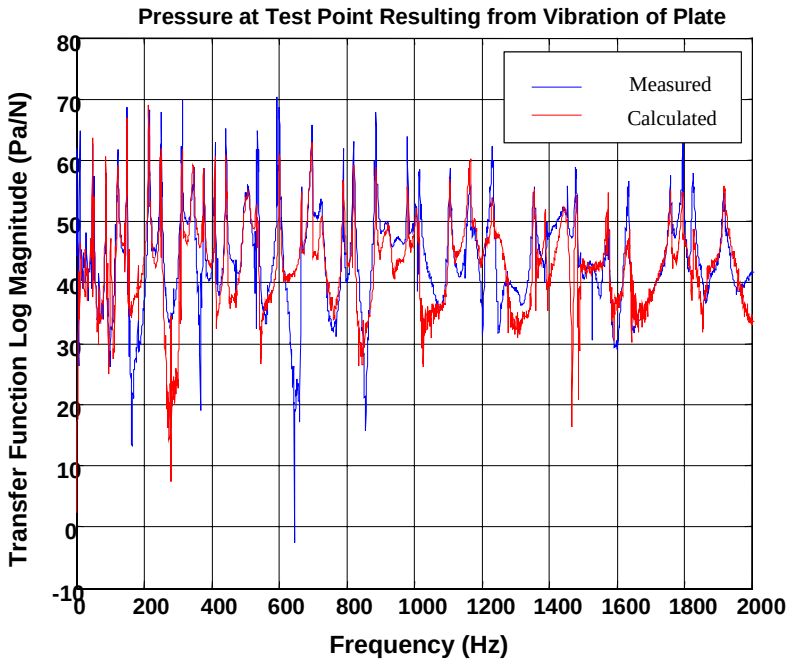

Figure 12: Comparison of measured and calculated radiated pressures

The measured and calculated transfer functions in figure 12 are satisfactorily similar. Notice, however, that there are two basic types of inconsistencies seen in this comparison: there are differences in the heights of the peaks, and there are discrepancies at low pressure levels. The differences in peak heights signify a difference in the amount of damping measured by the scanning vibrometer and the microphone. As mentioned before, this is due to the exponential windowing that was applied only to the vibrometer measurements and to the extremely low damping on the plate, which is difficult to measure precisely. There are also some discrepancies at low dB, but these are natural occurrences due to low system input level. As mentioned in the discussion of the exhaustive method, the radiation model simply adds a time delay and gain to the signal. It is important to notice from this comparison that the magnitude of the measured and calculated frequency responses are the same. Looking at a comparison of the measured and calculated pressures in the time domain will allow a check of the time delay.

The following (figure 13) is a comparison of the calculated and measured impulse responses from the input to a microphone about 1m from the plate (as in the frequency domain comparison above). While this view of the impulse response is too broad to see the initial time delay, it allows examination of the end of the impulse response. Notice

that the measured response rings longer than the pressure calculated using the exhaustive method. This is expected because of the damping level difference between the two transfer function measurements.

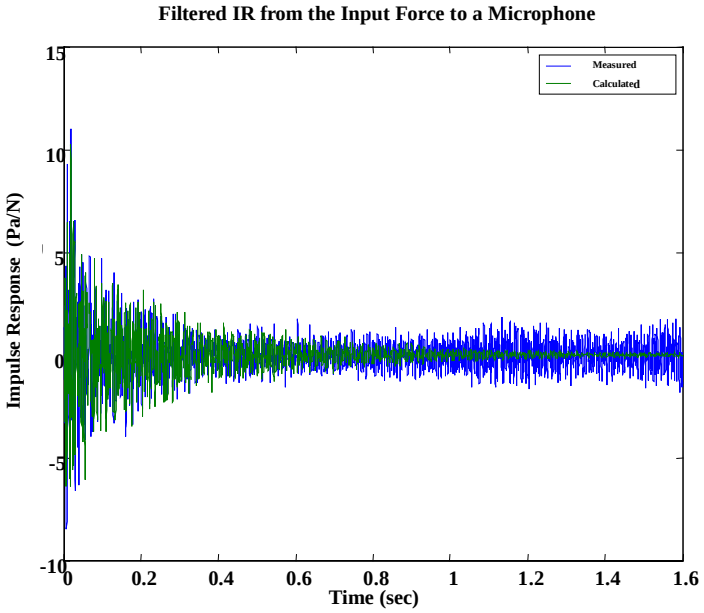

Figure 13: Extended time history of the impulse response

A closer view of the initial part of this impulse response (figure 14) shows good correlation between the time delay and magnitude of the impulse responses. This is significant because if there were any errors in the radiation model, there would be differences between the time delay and gain of the calculated and measured responses. The closely matching delay and magnitude verify that the radiation model part of the exhaustive method is correct.

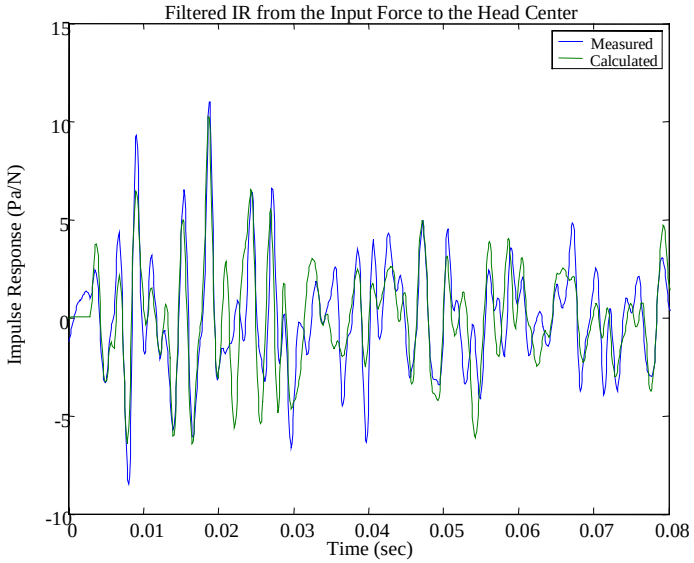

Figure 14: Close-up of impulse response

Verifying HRTF Application

In order to check the HRTF application part of the exhaustive method, the authors compared measured and calculated transfer functions between the input force and the binaural signals at the ears of a dummy head. The binaural signals were calculated with the plate velocities that were measured with the laser vibrometer as input to the exhaustive code (as with the radiation model check). The following discussion details how these calculated binaural signals compare to signals that were actually measured at the ears of a KEMAR dummy head.

Figure 15b shows the measured signal at the left ear of the KEMAR head compared with the left binaural signal calculated in the exhaustive method. As with the verification of the radiation model, there is good correlation between the time delay and magnitude of the measured and calculated impulse responses between the input force and the left ear (as shown in figure 15a).

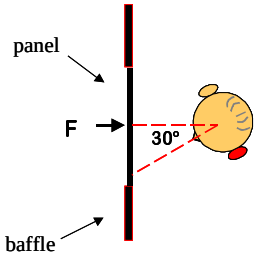

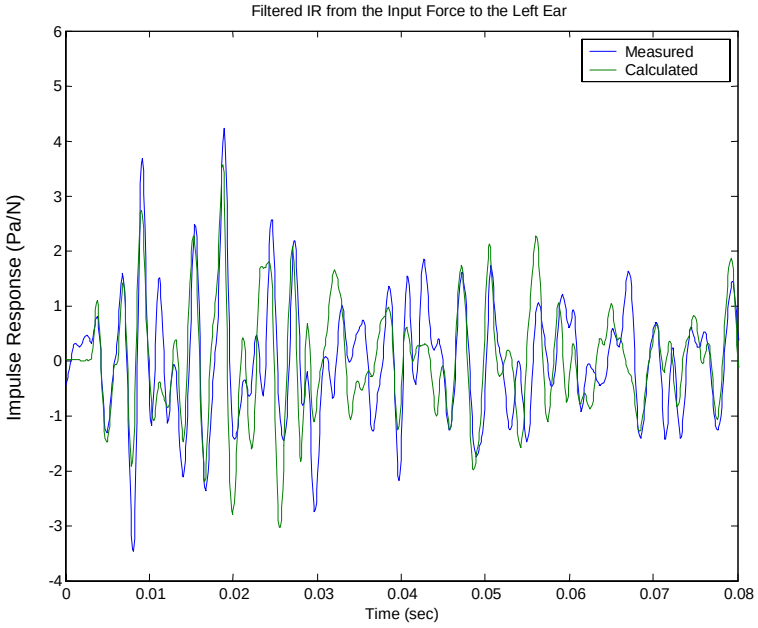

Figure 15a: Head orientation Figure 15b: Impulse response from input to left ear

Measurement Consistency

All of the above comparisons and validations are dependent upon the reliability of the collected data. The following plot (figure 16b) shows the transfer function from the input force to a reference microphone (positioned according to the configuration in figure 16a) during two separate tests. It is important to note that the position of the microphone was not changed at all between tests. Notice that the primary difference between the two measurements was simply the estimate of the damping. This is as expected because of the lightly damped nature of the plate and has been accounted for in the process of verifying the exhaustive method. As in previous comparisons, there are also some discrepancies at low dB, and this is also expected because there is a low signal to noise ratio at these frequencies.

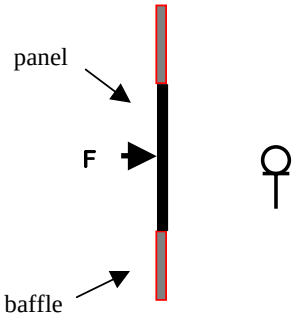

Figure 16a: Reference microphone configuration

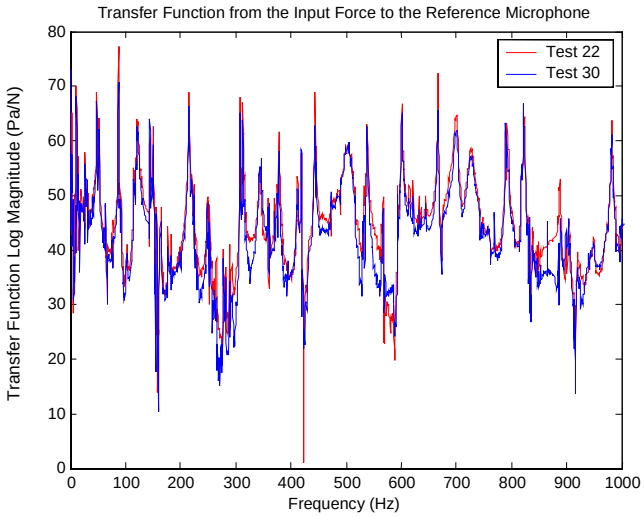

Figure 16a: Reference microphone transfer function

Wavenumber Decomposition

After verifying the consistency of measurements, the authors used wavenumber decomposition [18, 19] to find the frequency range for which the data is accurate. The plate was measured every 0.06m (figure 17a), which corresponds to a sample wavenumber of $k_s = 2\pi/\lambda = 102$ rad/m. Spatial aliasing will occur if the wavenumber on the plate is greater than half the sampling wavenumber. Figure 17b shows the wavenumber decomposition of the plate velocities at 550 Hz. At this frequency, the waves on the plate have wavenumbers mainly around $\boldsymbol{k} \approx 22$ rad/m, where k is defined according to equation 8:

$$k = \sqrt{k_x^2 + k_y^2} = \left[\frac{\omega^2 m}{D}\right]^{1/4} \tag{8}$$

Here D is defined as:

$$D = \frac{Eh^3}{12\left(1-\nu^2\right)} \tag{9}$$

where E is the modulus of elasticity of the plate, h is the plate thickness, and ν is the poisson's ratio of the plate.

Notice that the acoustic wavenumber, $k_a = \omega/c$ (which defines the wavenumber components that actually radiate sound from the plate) is only 10 rad/m, which is smaller than the structural wavenumber. This will become important in the discussion of wavenumber filtering later in the text. Figures 17c and 17d show the wavenumber

decomposition of the plate at 2000 and 4000 Hz respectively. In figure 17d aliasing is very visible, but at 2000 Hz (figure 17c) the bending wavenumber is equal to half the structural wavenumber, proving that the data is free of aliasing at frequencies up to 2000 Hz.

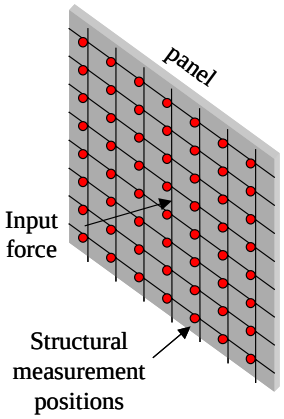

Figure 17a: Plate configuration

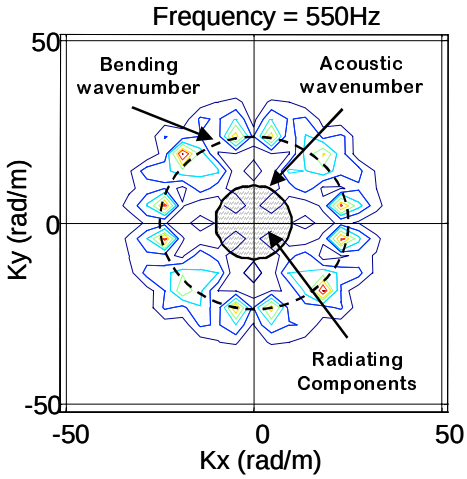

Figure 17b: Wavenumber decomposition at 500 Hz

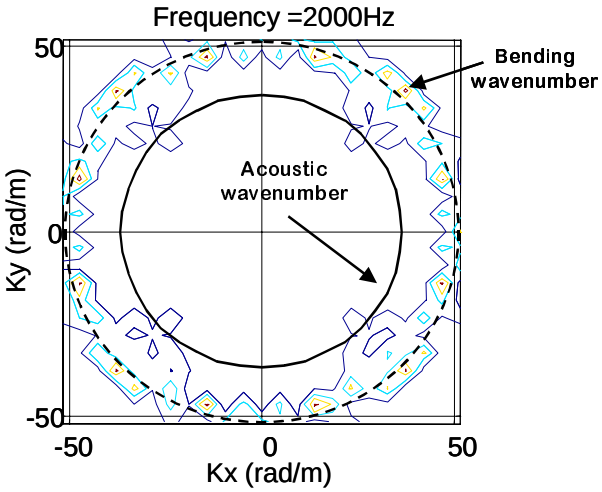

Figure 17c: Wavenumber decomposition at 2000 Hz

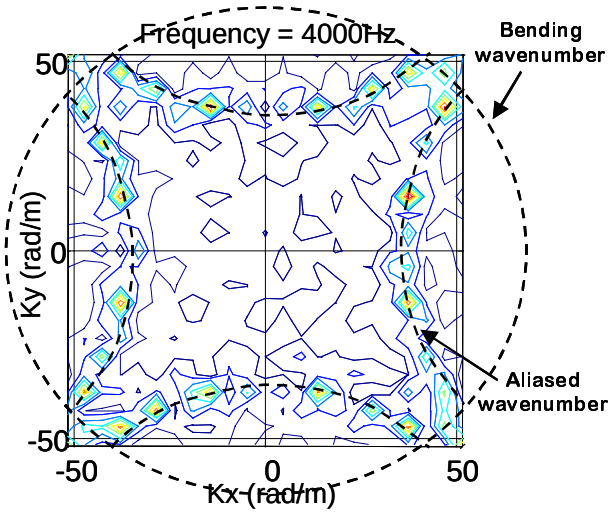

Figure 17d: Wavenumber decomposition at 4000 Hz

Reduction Methods

Having completed and verified the exhaustive method of calculating the binaural signals resulting from a structural acoustic source, the next step was to examine various methods for reducing the computing time and power required to make these calculations. Several reduction methods were examined, including: Wavenumber filtering, Equivalent Source Reduction, and Singular Value Decomposition. Of the three, wavenumber filtering was not used in this research. However, both Equivalent Source Reduction and Singular Value Decomposition were quite useful in reducing the amount of computations required. All three of these methods will be discussed, and a comparison will be made between the computations required in the SVD, ESR, and exhaustive methods.

Wavenumber Filtering

Recall the discussion concerning wavenumber decomposition in the exhaustive method section. In figure 18, the radiating components are defined as corresponding to the wavenumbers that are less than the acoustic wavenumber (in both the x and y direction). The theory behind wavenumber filtering is that since only some of the components radiate sound, for acoustic purposes it is only necessary to perform computations using these components [18, 19].

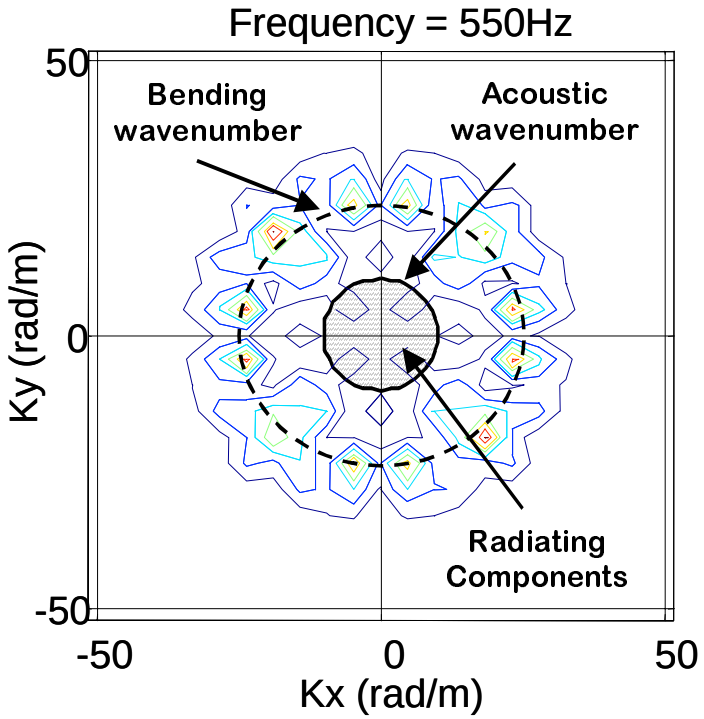

Figure 18: Wavenumber Decomposition of plate at 550 Hz

Wavenumber filtering (figure 19) is accomplished by first transforming velocity information from the spatial domain into the wavenumber domain via the Fourier transform. This signal is then low-pass filtered (with the cutoff at the acoustic

wavenumber) to isolate the radiating components. Next, the inverse Fourier transform is performed in order to transform the signal into the spatial domain. Finally, the signal is re-sampled at a lower "sample rate" (in quotations because sample rate typically refers to the time domain, whereas this analysis is done in the wavenumber domain, as previously mentioned).

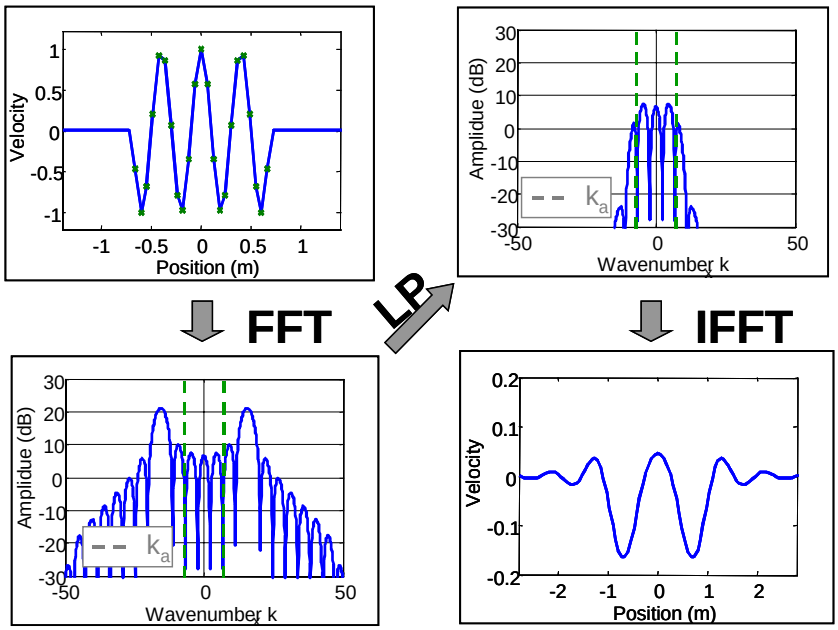

Figure 19: Wavenumber filtering

There are two main problems with this approach. First, the resampling process causes apparent sources to appear outside the actual edges of the plate. This is visible in the bottom right plot in figure 19, in which sources of velocity are seen as far as 2m from the center of the plate, which is outside the edges of the 1.4m by 1.4m plate. Second, wavenumber filtering can only be utilized for relatively simple geometries, such as a flat plate. For preliminary analysis, that is not an issue, but for more complex vibrating structures, such as the walls of the space station, wavenumber filtering will not be applicable. Since the future applications of this research include more complicated structures, wavenumber filtering will not be used. However, this is essentially what the equivalent source reduction method (next section) will achieve.

Equivalent Source Reduction

Another reduction method that was investigated is Equivalent Source Reduction. ESR effectively performs wavenumber filtering, but it can be used for more complex sources than wavenumber filtering and it does not create virtual sources outside the edge of the panel. Equivalent Source Reduction reduces the number of sources that are input into the exhaustive method (that is, N will be smaller in the exhaustive method schematic, figure 8).

Similar to wavenumber filtering, Equivalent Source Reduction reduces the number of computations by replacing the measurement points on the panel with a fewer number of equivalent sources. The equivalent sources are driven such that the radiated sound closely matches the original field. This is accomplished by creating an *evaluation surface* that is evenly covered by an array of *Q* evaluation points. For the case of a baffled plate radiating into a free field the evaluation surface is simply the far-field pressure (figure 20). At a single frequency, the far-field pressure can be described by a *Q* length vector, **p,** at the evaluation positions.

$$\mathbf{p} = \mathbf{T}\mathbf{a} \tag{10}$$

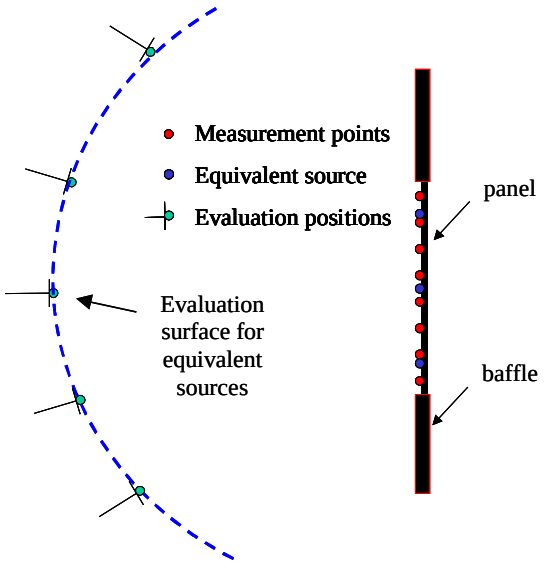

Figure 20: Evaluation surface of a baffled plate radiating sound into a closed room

The pressure is due to the acceleration of the *N* sources on the surface of the plate described by the vector **a**. The *Q* by *N* matrix of transfer functions, **T,** can be calculated from the frequency domain version of equation 4 [18,19]. The objective is to drive the N_E equivalent sources such that they accurately re-create the pressure at the evaluation surface.

$$\mathbf{p}_E = \mathbf{T}_E\mathbf{a}_E \tag{11}$$

The re-created pressure can also be calculated in a matrix form from the accelerations of the equivalent sources, $\mathbf{a_E}$. The *Q* by N_E transfer matrix, $\mathbf{T_E}$, is also calculated using the frequency domain version of equation 4. In order to minimize the differences between **p** and $\mathbf{p_E}$ a cost function *J* is developed.

$$J = (\mathbf{p} - \mathbf{p_E})^H(\mathbf{p} - \mathbf{p_E}) \tag{12}$$

This turns out to be a quadratic matrix problem with a unique minimum when [17, 22],

$$\mathbf{a_E} = \left[\mathbf{T_E^H T_E}\right]^{-1}\mathbf{T_E^H T a} = \mathbf{W a} \qquad (13)$$

The superscript *H* denotes the Hermitian or conjugate transpose. The term $\left[\mathbf{T_E^H T_E}\right]^{-1}\mathbf{T_E^H}$ is often called the pseudo-inverse of $\mathbf{T_E}$. This is performed at all of the frequencies of interest to create a matrix of filters, **W,** (in the frequency domain) that transform the accelerations, **a,** into the reduced set of accelerations, $\mathbf{a_E}$. By transforming the matrix of filters, **W,** into the time domain, the set of *N* time domain accelerations can be filtered into the reduced set of N_E equivalent accelerations (or sources). This can be done in a pre-processing stage before any real-time simulation is carried out.

For this technique to work well there must be (i) a sufficient number of evaluation positions (Q>N) and (ii) there must be at least two equivalent sources per *acoustic wavelength* whereas the measurements need to be every half of a *structural wavelength* (figure 21). Therefore, this technique will only be useful when the waves on the structure are predominantly subsonic (i.e. shorter than the acoustic wavelengths) as with the test plate below 2000Hz. It should be noted that the recreated acoustic field does not match the near-field of the original source accurately and will not produce good results close to the panel. However, virtual acoustic applications, in general, do not take into account the refractive effect of the head close to a source of a sound or the effect of near sources on the HRTFs. Therefore, it is thought that some inaccuracy can be tolerated in these circumstances.

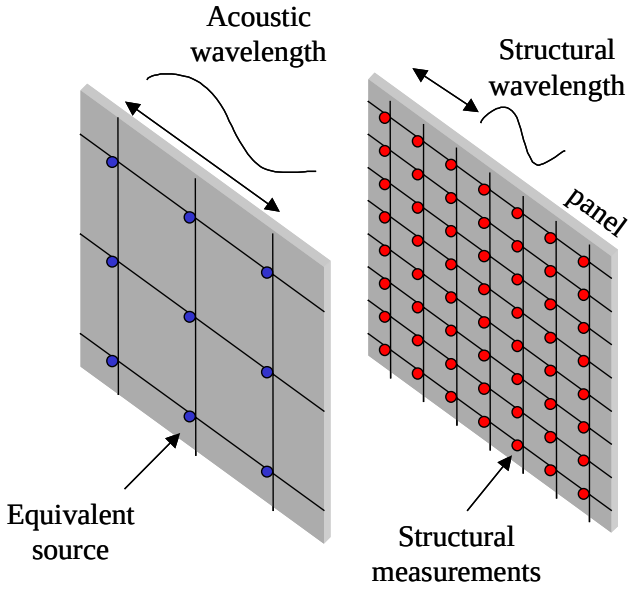

Figure 21: The equivalent source spacing depends on the acoustic wavelength

More generally, ESR can be applied to a more complex geometry by considering the velocity at the evaluation surface. Consider a closed surface S inside of which is an evaluation surface S_E (see figure 22). The particle velocity normal to the surface, S_E, due to the original set of sources of acceleration, **a,** is given by the Q length vector, **v**. If a set of equivalent sources, of acceleration $\mathbf{a_E}$, is driven such that it creates a particle velocity, $\mathbf{v_E}$, normal to the surface, S_E, that is the same as the velocity **v,** then the acoustic field inside the surface, S_E, will be the same as the original field. This can be deduced from the Kirchoff-Helmholtz equation [18, 19, 23].

$$\mathbf{v} = \mathbf{D}\mathbf{a} \tag{14}$$

$$\mathbf{v}_E = \mathbf{D}_E\mathbf{a}_E \tag{15}$$

$$J = (\mathbf{v} - \mathbf{v_E})^H(\mathbf{v} - \mathbf{v_E}) \tag{16}$$

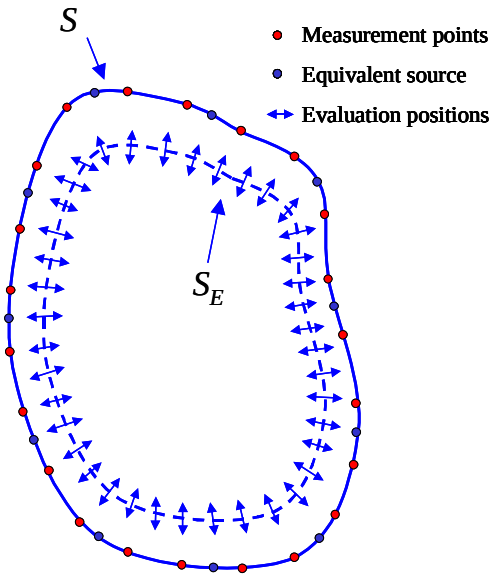

Figure 22: Evaluation surface enclosed within a closed radiating surface

In this example the velocity at the evaluation surface now becomes a function of the dynamic (or modal) behavior of the space and this is taken into account in the calculation of the transfer matrices **D** and $\mathbf{D_E}$. The optimal set of equivalent source strengths can be calculated using the pseudo-inverse as,

$$\mathbf{a_E} = \left[\mathbf{D_E^H D_E}\right]^{-1}\mathbf{D_E^H D a} \tag{17}$$

This method will be effective as long as the listener in the simulation is inside of the surface, S_E (this is similar to the near-field problem discussed before). In this example there is no restriction on where the equivalent sources are placed as long as they lie outside of the surface S_E. The calculation of the matrices **D** and $\mathbf{D_E}$ can be undertaken

using boundary element methods or other equivalent source modeling techniques. The ESR method can also be applied to surfaces that make up only a part of the total surface, as shown in figure 23. Under these circumstances the evaluation surface only encloses the section of the surface that is vibrating.

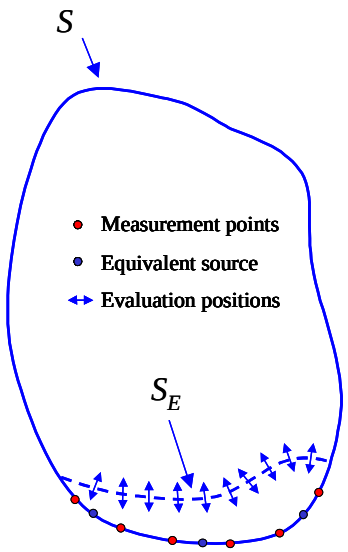

Figure 23: The evaluation surface encloses only the vibrating section of the surface

Having determined that ESR was a promising reduction method, the authors implemented the exhaustive method using the reduced number of equivalent sources. Similar to the checks on the exhaustive method, two comparisons were made. The pressure at a microphone in space was calculated through the exhaustive method and the equivalent source method, and these two pressures were compared. (Note: the equivalent source schematic is the same as the exhaustive method, except that the number of input sources, *N*, is reduced). These two methods were also used to find and compare the binaural signal at the left ear of a KEMAR head.

Figure 24 shows a far-field comparison of the pressure spectra at a microphone in space. Notice that the 8 by 8 grid of replacement sources matches the original 23 by 23 grid of sources at frequencies up to 980 Hz. This is expected because the source spacing (0.176m) is equivalent to half an acoustic wavelength ($\pi c/\omega$) at 980 Hz.

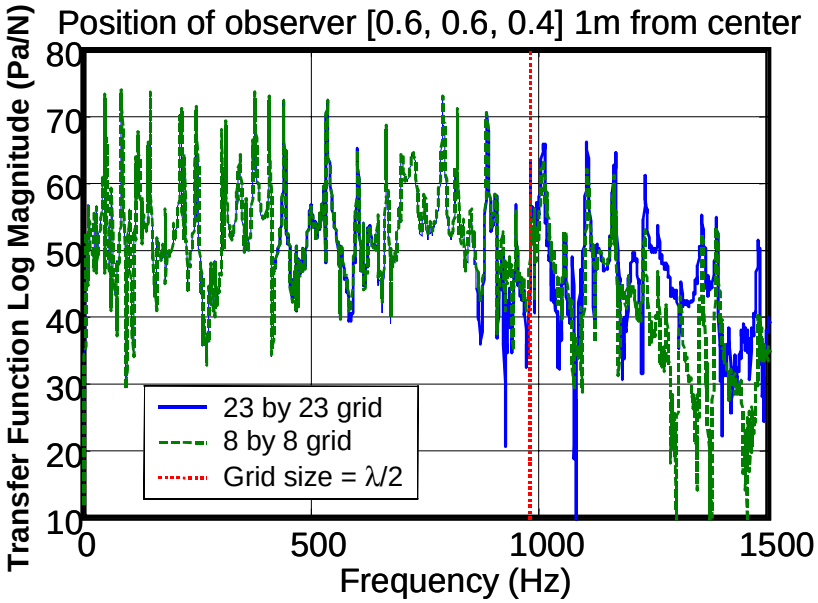

Figure 24: Pressure at observer calculated through exhaustive and ESR methods

Notice that in the near-field (figure 25) the equivalent source method is not as accurate. The two pressure signals will diverge even further after HRTFs are applied in order to calculate the binaural signals.

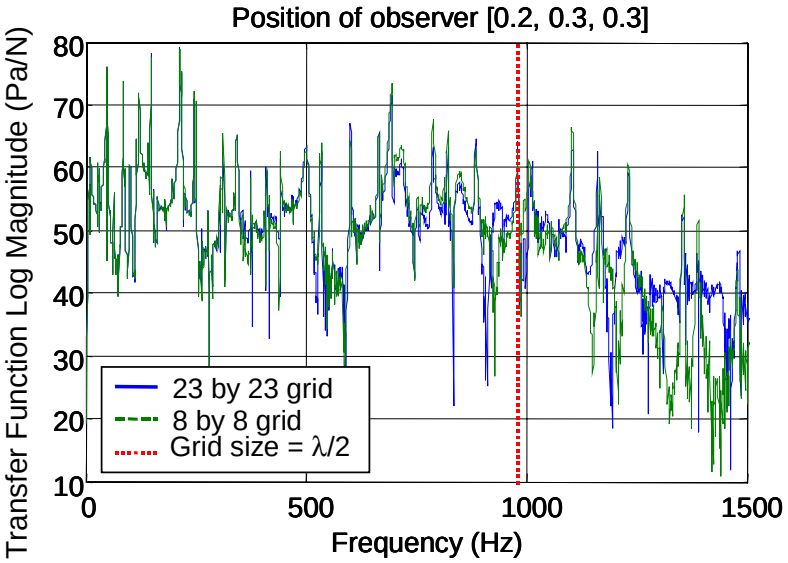

Figure 25: Pressure at close observer calculated through exhaustive and ESR methods

When only 16 equivalent sources (figure 26) are used, this method is accurate up to 490 Hz. Again, this is because the source spacing is equal to half the acoustic wavelength at 490 Hz.

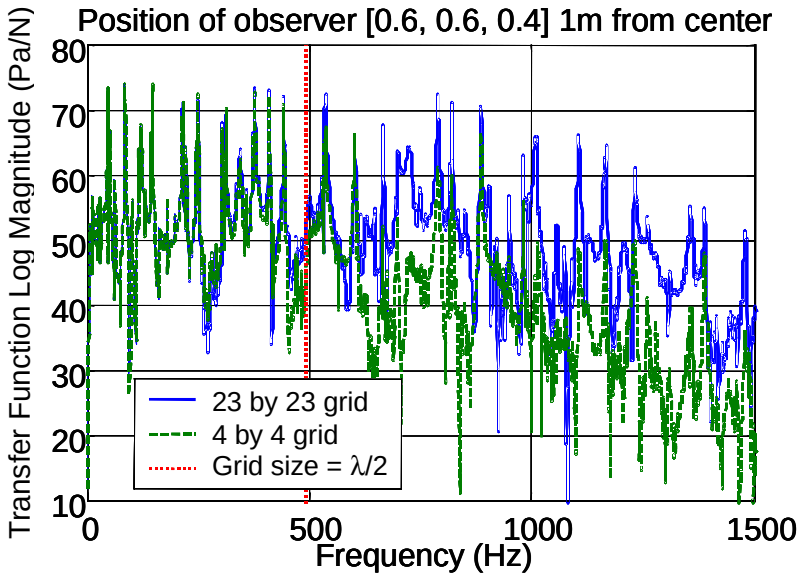

Figure 26: Pressure at observer calculated by exhaustive and 16 source ESR methods

The following figure (27b) shows the frequency domain comparison of the pressure at the left ear of a listener (configuration in figure 27a). Notice that with 64 sources, the ESR method is very close to the exhaustive method up to about 1000 Hz.

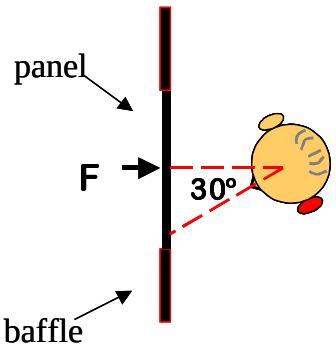

Figure 27a: Head orientation

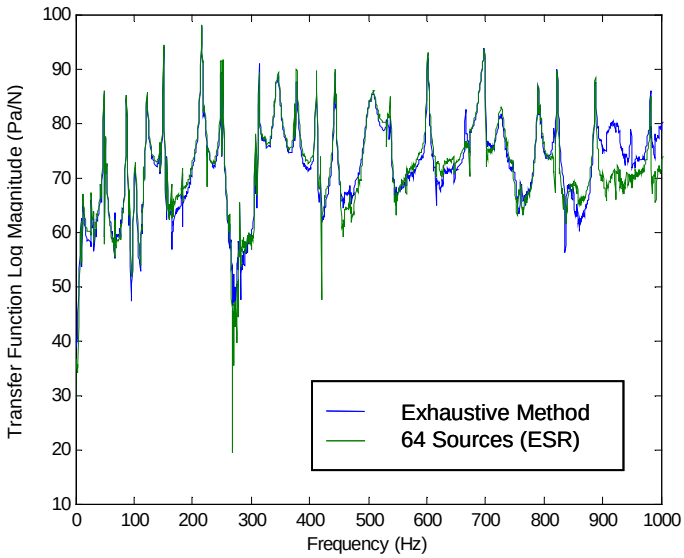

Figure 27b: Calculated pressure at left ear

Figure 28 depicts the time domain version of figure 27b (low-pass filtered at 800 Hz). Cross-correlation of these two signals yields a correlation of 98.4%.

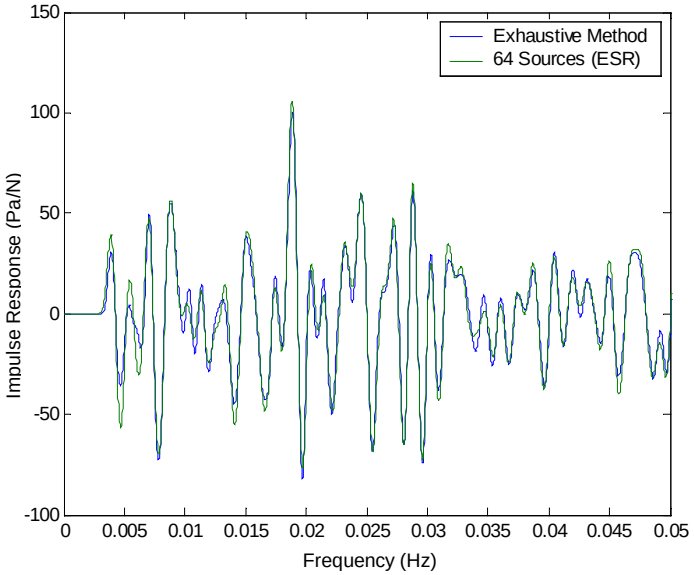

Figure 28: Calculated pressure at left ear

When only 16 sources are used, the frequency domain version of the left binaural signal (configuration in figure 27a) that was calculated using the ESR method is accurate up to 490 Hz (figures 29 and 30).

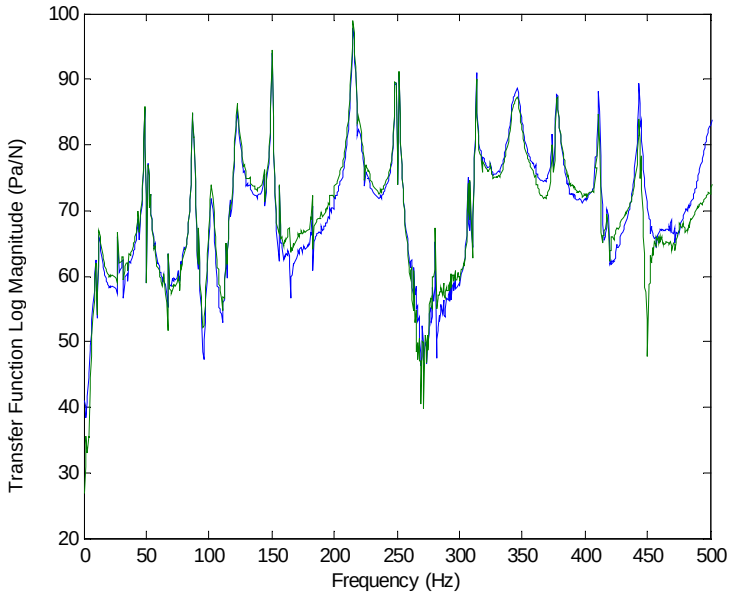

Figure 29: Left Binaural Signal in Frequency Domain

In the time domain (with a low-pass filter at 400 Hz), the correlation is found to be 98%.

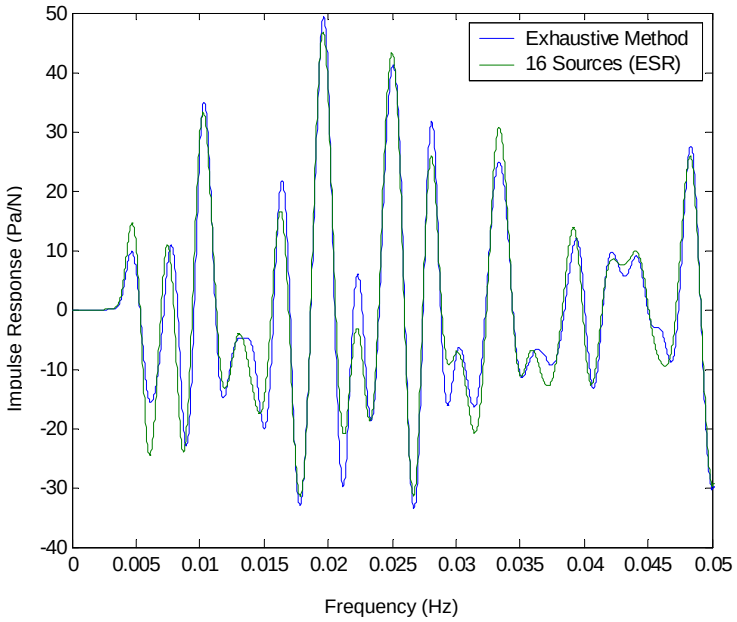

Figure 30: Left Binaural Signal in Time Domain

Singular Value Decomposition

A third reduction method investigated was singular value decomposition [23]. By breaking down the matrix of HRTFs into three separate matrices, the number of convolutions can be greatly reduced. Since convolution is computationally expensive, a great deal of processing time can be avoided by a small amount of pre-processing. This discussion will describe how singular value decomposition works, how it applies to the exhaustive method, and the comparisons that were made to verify that the SVD method is accurate.

Singular value decomposition is simply separating a matrix (in this case a matrix of HRTFs) into three separate matrices: **U**, **Σ**, and **V** (equation 18).

$$HRTFs = U * \Sigma * V^T \tag{18}$$

U is a matrix of left singular vectors, **Σ** is a diagonal matrix of singular values, and **V** is a matrix containing right singular vectors. The relative sizes of these matrices are visible in figure 31. It is important to note that singular value decomposition of the HRTF matrix can be done in either the time or frequency domain, but for the following analysis, the SVD was performed on a matrix of HRTFs in the time domain.

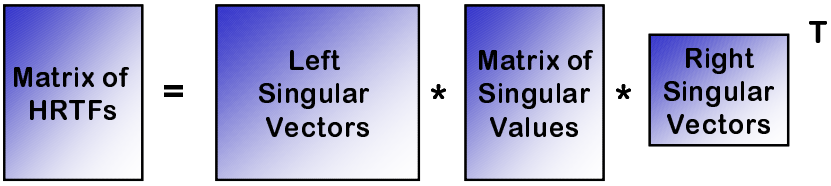

Figure 31: Singular Value Decomposition of the HRTF matrix

The original matrix of HRTFs for the left ear at 0° elevation is shown below in figure 32. Notice that when the sound approaches the left ear directly (angle between directly ahead and the approach of the sound is 90°) the sound is loud and contains high frequency content. When the sound comes from the other side of the head (-90°), the sound level is lower (due to the IID), there is a time delay (ITD), and the signal contains mostly low frequencies because higher frequencies are shadowed by the head.

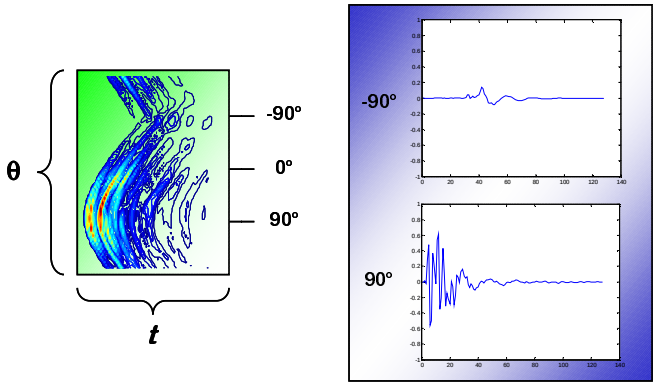

Figure 32: Time Domain HRTFs for 0° elevation

The first step taken in the SVD method was to create a function to describe the time delay of the HRTFs for each angle and remove that time delay from each impulse response in the matrix of HRTFs (figure 33). This time delay removal causes the matrix of HRTFs to be a smoother angular function so that the singular value decomposition can be performed with greater accuracy. Note that this operation is not necessary for HRTFs having a minimum phase representation. The time delay removed in this operation is added to the retarded time delay (r/c) in the radiation model.

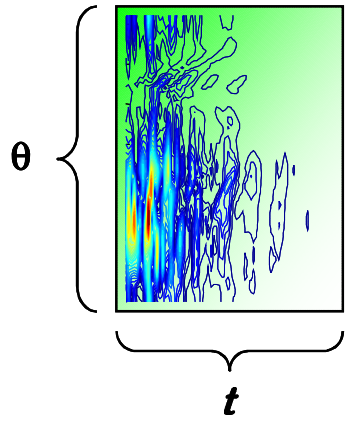

Figure 33: Time domain HRTFs with ITD removed

The singular value decomposition of the HRTF matrix (without time delays) is shown below in figure 34. Notice that the left singular vector matrix contains angular information for each singular value σ_i. The matrix of singular values is simply a diagonal matrix of singular values, which diminish in value as *i* becomes larger. Time information per singular value is contained in the right singular vector matrix. When these three matrices are multiplied together, the matrix of HRTFs (without time delays) will be the result. The advantage of SVD is that an approximate HRTF matrix can be obtained using only a few singular values. This will become important as the SVD process is applied to the exhaustive method.

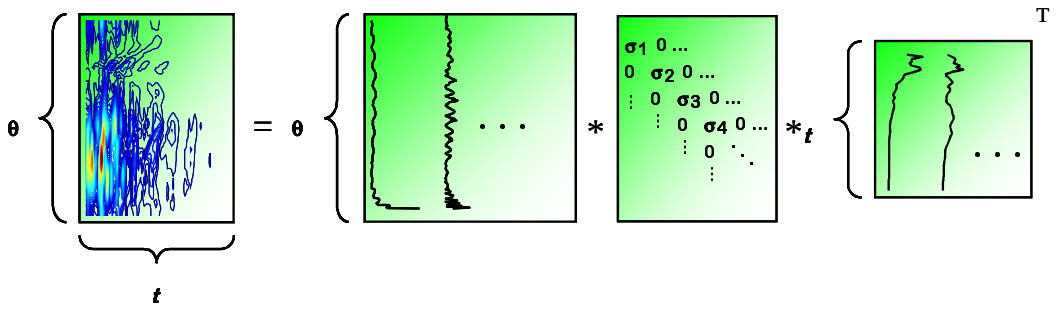

Figure 34: SVD of time domain HRTFs

Recall the schematic of the exhaustive code in figure 8. Shown below is a similar schematic of the SVD reduction method (figure 35). Note that instead of simply convolving the HRTFs with the radiated pressure for each of the *N* sources, the SVD method expands the application of the HRTFs into four faster operations that are performed for each of *M* important singular values. The first operation is a scalar multiplication (radiated pressure times *U(i)* for *i* = 1:*M*) for each of the *N* sources. The signals are then summed and convolved only *M* times with the right singular vectors (*V(i)* for *i* = 1:*M*). Each filtered signal is then multiplied by its singular value, σ, and then summed to produce the left ear signal (a similar process is carried out for the right ear

signal). Notice that this method is more complicated than the exhaustive method and there is no advantage to the SVD method unless *M* is much smaller than *N*.

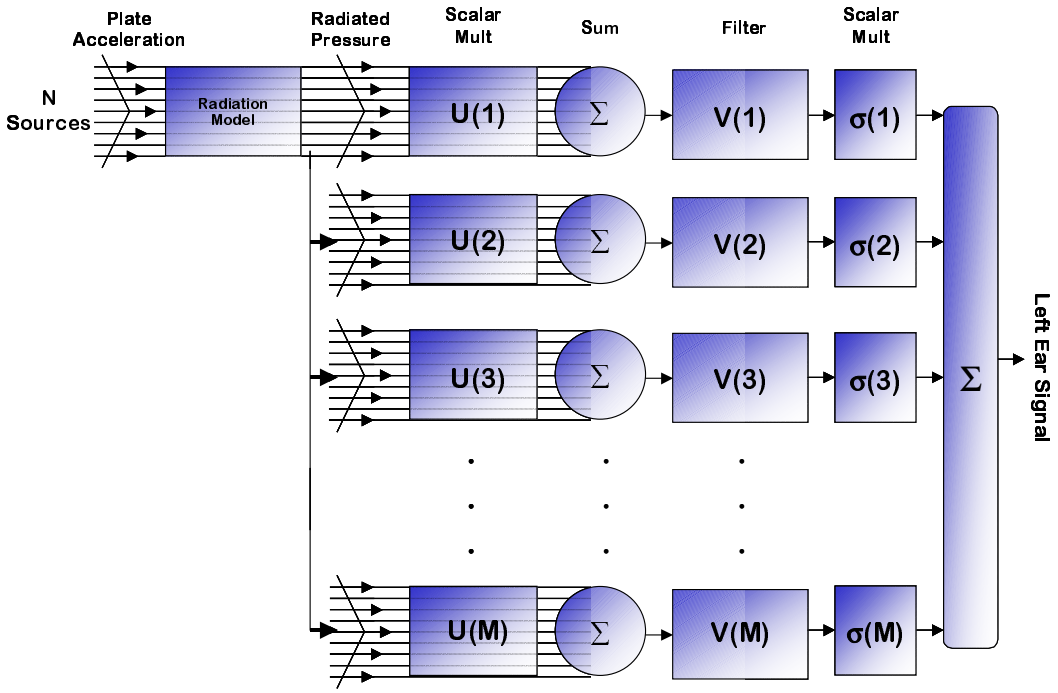

Figure 35: Schematic of the SVD method

So how many singular values really are important? Depending on how the HRTFs are pre-processed before SVD is performed, the value of the singular values will drop off slower or faster. Figure 36 shows a plot of the singular values under four different circumstances. In the first case, the SVD is executed on the HRTFs over the entire frequency range. In the second case, the HRTFs are logarithmically weighted according to frequency before performing the SVD. This applies more weight to lower frequencies since humans detect sound on a logarithmic scale. After performing the SVD, the logarithmic weighting is removed. The third scenario applies logarithmic weighting and low-pass filters the sound at 2000 Hz. Lastly, the sound is logarithmically weighted and low-pass filtered at 5000 Hz. Notice that the level of the singular values falls more sharply for smaller frequency ranges. This makes logical sense because it takes fewer singular values to reproduce a signal that contains less frequency information. The number of important singular values, then, is dependent upon the criterion used. The authors selected a 25 dB criterion, choosing to use three singular values. The real criterion in selecting the number of important singular values is the correlation between the SVD method and the exhaustive method, which will be discussed next.

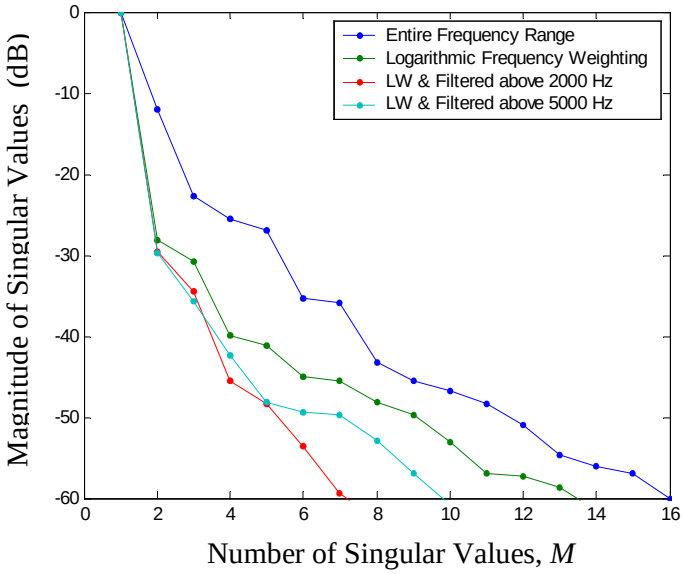

Figure 36: Number of important singular values

Figure 37b depicts the transfer function from the input force to the left ear (as shown in figure 37a) and compares this transfer function as it is calculated with the exhaustive and SVD methods (three singular values were used). Note that there is very good agreement between the two and that any discrepancies occur at low dB. A more concrete comparison can be made in the time domain, however.

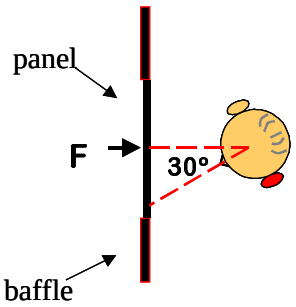

Figure 37a: Head orientation

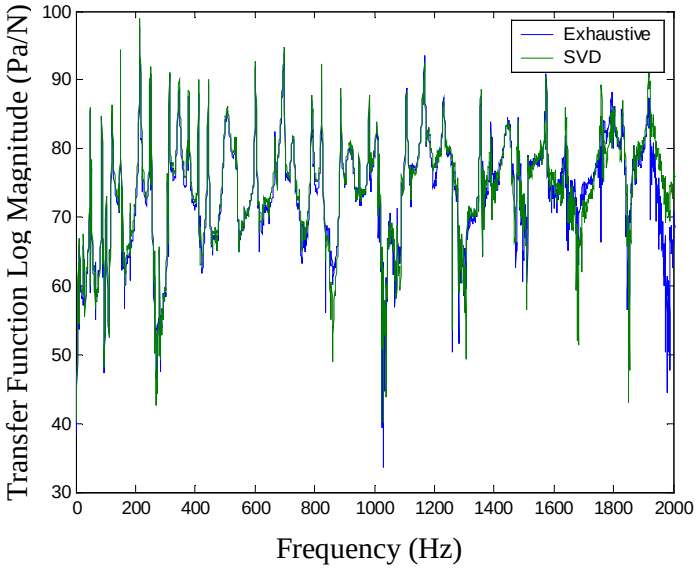

Figure 37b: Calculated pressure at left ear

Figure 38 shows the same transfer function from the input force to the left ear as shown above, but in the time domain. Since the data is only good up to 2000 Hz, a low-pass filter at 1600 Hz was applied. The correlation between the SVD (only 3 singular values used) and exhaustive methods was a remarkable 97.7%. From this result the authors concluded that singular value decomposition is an accurate reduction method and can be effectively used in this research.

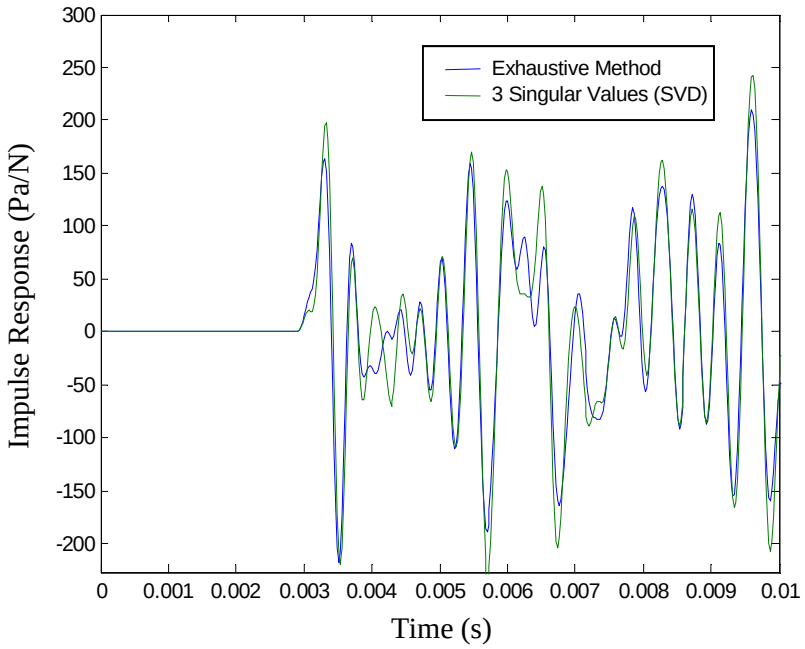

Figure 38: Impulse response between input force and left ear

ESR and SVD Together

Since the ESR method works to reduce the number of input sources while the SVD method changes how HRTFs are applied, the two methods can be used simultaneously to yield an even greater reduction in computation time. Figure 39 shows a time domain comparison of the combined reduction methods and the exhaustive method. In this case, three singular values and an eight by eight grid of equivalent sources were used. Because the ESR method for an eight by eight grid is only accurate up to 980 Hz, a low-pass filter at 800 Hz was applied. A correlation of 97% was found between the combined reduction method and the exhaustive method. This level of accuracy is sufficient to conclude that the combined reduction method can be effectively used in this research.

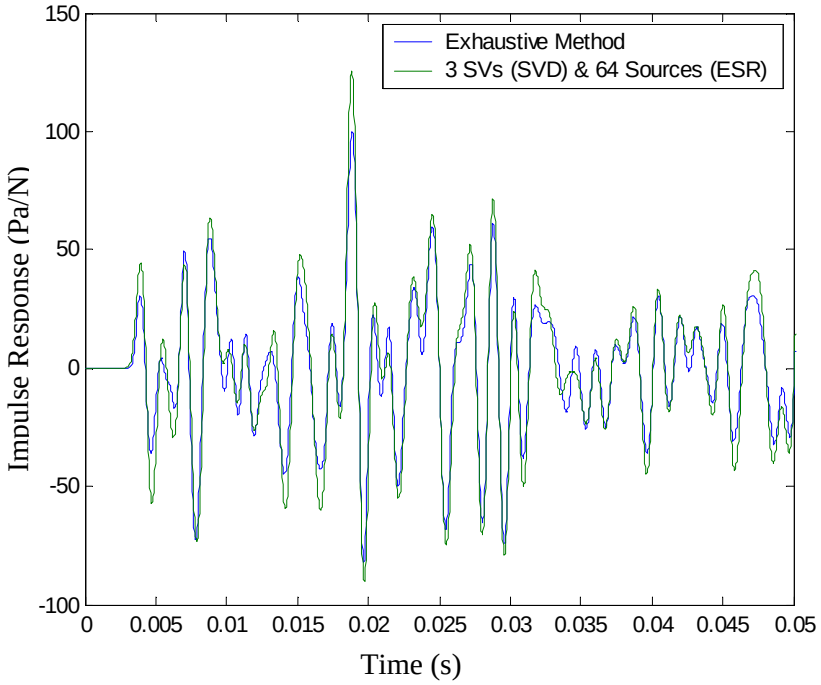

Figure 39: Impulse response between input force and left ear

Computation Time

Now that it has been verified that the ESR, SVD, and combined reduction methods can accurately replace the exhaustive method, it remains to determine if these methods actually reduce the number of computations in this analysis. To handle this problem, the authors developed an estimate of the computation time required for each method that is based solely upon the number of additions and multiplications used in each method.

The schematic of the exhaustive method is shown below in figure 40. Since the radiation model process is scalar multiplication, the number of computations is modeled to be *N* multiplications. Convolution is required in the process of filtering the radiated pressure with the HRTFs, so the number of computations required will be 128**N* multiplications plus 128**N* additions. Summing the *N* components of the left ear signal is simply *N* summations. In this model, addition and multiplication are estimated to require approximately the same amount of computation time. Adding up the number of summations and multiplications required by the exhaustive method yields a total of 258*N computations. In the case of the original plate, with a 23 by 23 grid of measurement points, the total number of computations would be 136,482.

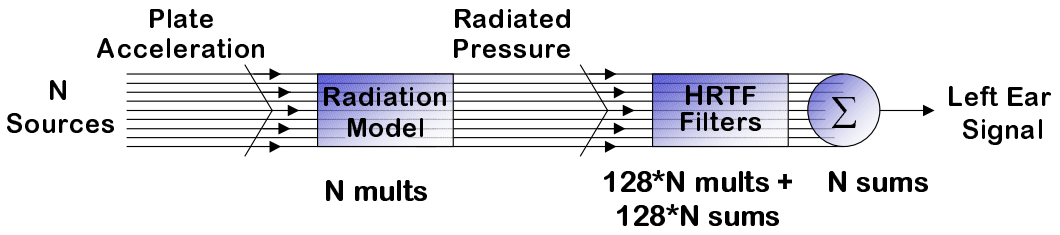

Figure 40: Computation time schematic of the exhaustive method

In the case of the ESR method, the schematic is the same as in figure 40. The difference is found in the number of sources (*N*). For a model with 64 sources (which is accurate up to 980 Hz), the number of computations will be 16,512. If only 16 sources are used, the number of calculations would be reduced to 4128, but the data is only accurate up to 490 Hz. There is an obvious reduction in computation time achieved using the ESR method, but there is a tradeoff involving the frequency range of accuracy.

The reduction in computation time achieved with the SVD method is less intuitive because the system is more complex (figure 41). The computations required by the radiation model, though, are the same as with the ESR method: *N* multiplications. Multiplying the left singular vector, *U(i)*, requires *N* multiplications for each of the *M* singular values, which is *M*N* multiplications. By the same reasoning, the summing process requires *M*N* summations. Since the convolution occurs after the summing process in the SVD method, only *M*128* multiplications and *M*128* additions are required. The scalar multiplication of the singular values is not included in the number of computations because it can be multiplied by the right singular vectors in pre-processing. The total number of computations is $N + 2MN + 257M$, which is 4474 computations if three singular values and 529 input sources are used.

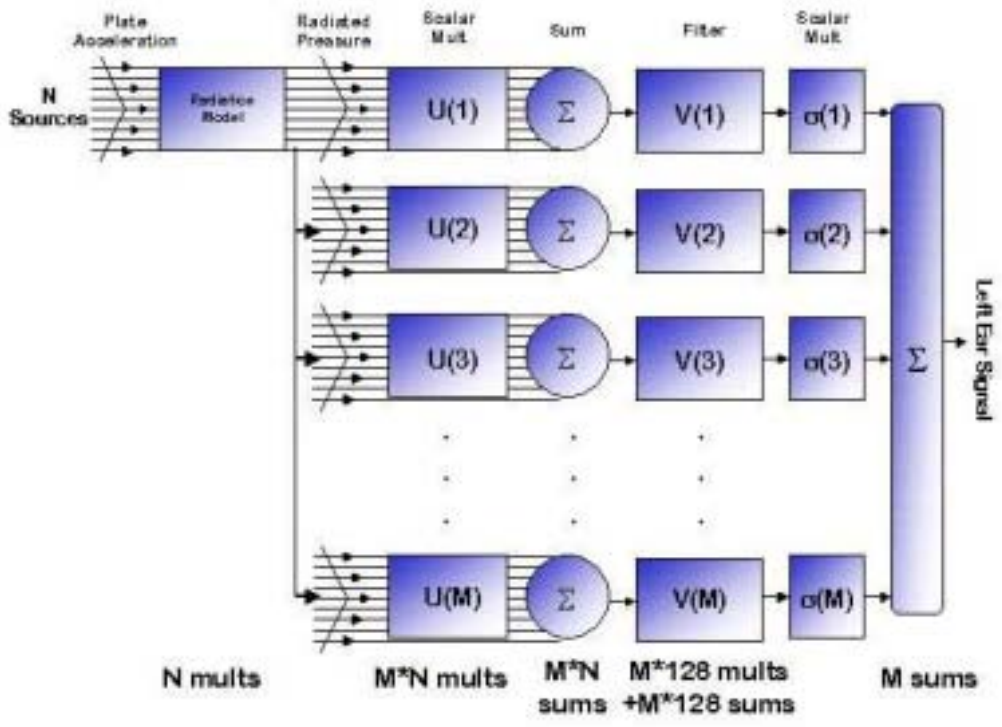

Figure 41: Computation time schematic of the SVD method

If ESR is combined with the SVD method, the number of input sources can be reduced to 64 sources, for example. In that case, the total number of computations would be 1219. When compared with the 136,482 computations required by the exhaustive method, (even though this model is only an approximation) it is safe to conclude that the ESR, SVD, and combination methods all produce significant reduction in the required number of computations and in turn, processing time. Table 1, below, offers a comparison of the computation time associated with each method.

Table 1: Computations required by exhaustive and reduction methods

Method	M	N	Freq. Limit (Hz)	# comps
Exhaustive	N/A	529	N/A	**136482**
ESR	N/A	64	980	**16512**
ESR	N/A	16	490	**4128**
SVD	7	529	N/A	**9734**
SVD	3	529	N/A	**4474**
ESR & SVD	7	64	980	**2759**
ESR & SVD	7	16	490	**1911**
ESR & SVD	3	64	980	**1219**
ESR & SVD	3	16	490	**883**

This reduction in computation time is important in order to create a real-time binaural simulation of structural acoustic data. In a real-time virtual environment, the user's head orientation is measured by a head-tracking unit and fed into the computer. Typical update rates for head-tracking units are 100 Hz corresponding to one update every 10 ms. Until the computer receives another head orientation from the head-tracking unit, the left and right ear signals are calculated based upon the current head orientation. However, the audio and visual outputs are also based on other inputs. For instance, if the simulation were of a jet flying overhead, the sound input from the simulated jet would be updated at a sample rate of 44100 samples/second. This means that in order to create a structural acoustics simulation using the exhaustive method, the computer must make an estimated 136,482 calculations per ear in about 23 μs. With the combined reduction methods, only 883 calculations are required per ear in the same amount of time. This is an estimated computation time reduction of 99.4%, making real-time binaural analysis of structural acoustic data a possibility.

Conclusion

The goal of this research has been to reduce the computation time required in calculating the binaural signals to reproduce the sound radiated from a vibrating structure. This was accomplished by developing an exhaustive method to calculate the binaural signals and by verifying that method through a comparison of the results with actual data. Several reduction methods were investigated and the ESR and SVD methods showed exceptional promise. These two methods were tested by implementing the necessary changes to the computer code for the exhaustive method. The results were compared with those in the exhaustive method and found to have high correlations. In addition, the two reduction methods can also be combined since each method's changes affect different portions of the calculation process. The only limiting factor with either method is that the ESR method has a frequency range of accuracy that depends upon the spacing of the equivalent sources. After the accuracy of the reduction methods was determined, the computation time required by each method was estimated. It was found that the ESR, SVD, and combined reduction methods all accurately replace the exhaustive method for calculating structural acoustic binaural signals while significantly reducing the estimated computation time.

Future Work

While there is excellent correlation between the results from the reduction methods and the exhaustive methods in objective tests, this analysis could be supported in the future with auditory tests. Some preliminary tests have been performed, but more scientific tests involving several subjects would enhance the results of this research. In addition, the effects of an acoustic enclosure and more complex geometries have yet to be investigated.

Another improvement to this research would be to use individualized HRTFs instead of generalized ones. The largest amount of error introduced into each method is probably the use of generalized HRTFs, because each person has differently shaped heads and torsos. Using individualized HRTFs would minimize that error, allowing listeners in auditory tests to distinguish small errors. Since the reduction methods cause smaller errors than that of the generalized HRTFs, this would greatly improve the validity of auditory tests.

Acknowledgements

The authors would like to gratefully acknowledge the help of Dr. Stephen A. Rizzi and Brenda M. Sullivan of the NASA Langley Research Center and Dr. Ferdinand W. Grosveld of the Lockheed Martin Engineering and Sciences Company in Hampton, VA.

Bibliography

[1] Begault, D., *3-D Sound for Virtual Reality and Multimedia* (Boston: Academic Press, 1994).

[2] Cheng, C.I., and G.H. Wakefield, "Introduction to Head-Related Transfer Functions (HRTF'S): Representations of HRTF's in Time, Frequency, and Space (invited tutorial)," *Proceedings of the 107th Audio Engineering Society (AES) Convention* (1999).

[3] Martens, W.L., "Principal Components Analysis and Resynthesis of Spectral Cues to Perceived Direction," *1987 ICMC Proceedings* (1987), pp. 274-281.

[4] Kistler, D.J. and F.L. Wightman, "A Model of Head-Related Transfer Functions Based on Principal Components Analysis and Minimum-Phase Reconstruction," *Journal of the Acoustical Society of America*, vol. 91, no. 3 (1992), pp. 1637-1647.

[5] Chen, J., B.D. Van Veen, and K.E. Hecox, "A Spatial Feature Extraction and Regularization Model for the Head Related Transfer Function," *Journal of the Acoustical Society of America*, vol. 97, no. 1 (Jan. 1995), pp. 439-452.

[6] Wu, Z., F.H.Y. Chan, F.K. Lam, and J.C.K. Chan, "A Time Domain Binaural Model Based on Spatial Feature Extraction for the Head-Related Transfer Function," *Journal of the Acoustical Society of America*, vol. 102, no. 4 (Oct. 1997), pp. 2211-2218.

[7] Mackenzie, J., J. Huopaniemi, V. Valimaki, and I. Kale, "Low-Order Modeling of Head-Related Transfer Functions Using Balanced Model Truncation," *IEEE Signal Processing Letters*, vol. 4, no. 2 (Feb. 1997), pp. 39-41.

[8] Georgiou, P.G., and C. Kyriakakis, "Modeling of Head Related Transfer Functions for Immersive Audio Using a State-Space Approach," *Conference Record of the Thirty-Third Asilomar Conference on Signals, Systems & Computers*, vol. 1 (1999), pp. 720-724.

[9] Georgiou, P.G., A. Mouchtaris, S.I. Roumeliotis, and C. Kyriakakis, "Immersive Sound Rendering Using Laser-Based Tracking," *Proceedings of the 109th Audio Engineering Society (AES) Convention*, preprint No. 5227 (Sept. 2000).

[10] Evans, M.J., J.A.S. Angus, and A.I. Tew, "Analyzing Head-Related Transfer Function Measurements Using Surface Spherical Harmonics," *Journal of the Acoustical Society of America*, vol. 104, no. 4 (Oct. 1998), pp. 2400-2411.

[11] Nelson, P.A., and Y. Kahana, "Spherical Harmonics, Singular-Value Decomposition and the Head-Related Transfer Function," *Journal of Sound and Vibration*, vol. 239, no. 4 (2001), pp. 607-637.

[12] Jenison, R.L., “A Spherical Basis Function Neural Network for Pole-Zero Modeling of Head-Related Transfer Functions,” *IEEE ASSP Workshop on Applications of Signal Processing to Audio and Acoustics* (Oct. 1995).

[13] Runkle, P.R., M.A. Blommer, and G.H. Wakefield, “A Comparison of Head Related Transfer Function Interpolation Methods,” IEEE ASSP Workshop on Applications of Signal Processing to Audio and Acoustics, IEEE catalog No. 95TH8144 (Oct. 1995).

[14] Brown, C. P., and R. O. Duda, "A Structural Model for Binaural Sound Synthesis," *IEEE Trans. on Speech and Audio Processing*, vol. 6, no. 5 (Sept. 1998), pp. 476-488.

[15] Brown, C.P., and R.O. Duda, “An Efficient HRTF Model for 3-D Sound,” *1997 IEEE ASSP Workshop on Applications of Signal Processing to Audio and Acoustics* (Oct. 1997).

[16] Duda, R.O., “Modeling Head Related Transfer Functions,” *Proc. Twenty-Seventh Asilomar Conference on Signals, Systems and Computers* (Oct. 1994), pp. 457-461.

[17] Johnson, M. E., S. J. Elliott, K-H Baek, and J. Garcia-Bonito, “An Equivalent Source Technique for Calculating the Sound Field Inside an Enclosure Containing Scattering Objects,” *Journal of the Acoustical Society of America*, vol.104, no. 3 (1998), pp. 1221-1231.

[18] Fahy, F., *Foundations of Engineering Acoustics*, 1st ed. (New York: Academic Press, 2001), p. 110.

[19] Fahy, F., *Sound and Structural Vibration: Radiation, Transmission and Response*, 1st ed. (New York: Academic Press, 1985), pp. 56, 60-89.

[20] Gardner, W.G., and K.D. Martin, “HRTF Measurements of a KEMAR”, *Journal of the Acoustical Society of America*, vol. 97, no. 6 (June 1995), pp. 3907-3908.

[21] Grosveld, F.W., “Binaural Simulation Experiments in the NASA Langley Structural Acoustics Loads and Transmission Facility, NASA/CR-2001-211-255, *http://techreports.larc.nasa.gov/ltrs/PDF/2001/cr/NASA-2001-cr211255.pdf* (Hampton: NASA Langley Research Center, Dec. 2001).

[22] Nelson, P. A. and S.J. Elliott, *Active Control of Sound* (New York: Academic Press, 1993).

[23] Kung, S., “A New Identification and Model Reduction Algorithm Via Singular Value Decompositions,” *Conference Record of the Twelfth Asilomar Conference on Circuits, Systems and Computers* (Nov. 1978), pp. 705-714.

REPORT DOCUMENTATION PAGE

Form Approved
OMB No. 0704-0188

1. AGENCY USE ONLY *(Leave blank)*	2. REPORT DATE	3. REPORT TYPE AND DATES COVERED
	July 2002	Contractor Report

4. TITLE AND SUBTITLE
Development of an Efficient Binaural Simulation for the Analysis of Structural Acoustic Data

5. FUNDING NUMBERS
NCC1-01029
705-30-11-13

6. AUTHOR(S)
Aimee L. Lalime
Marty E. Johnson

7. PERFORMING ORGANIZATION NAME(S) AND ADDRESS(ES)
Vibrations and Acoustics Laboratories
Department of Mechanical Engineering
Virginia Polytechnic Institute and State University
Blacksburg, VA 24061

8. PERFORMING ORGANIZATION REPORT NUMBER

9. SPONSORING/MONITORING AGENCY NAME(S) AND ADDRESS(ES)
National Aeronautics and Space Administration
Langley Research Center
Hampton, VA 23681-2199

10. SPONSORING/MONITORING AGENCY REPORT NUMBER
NASA/CR-2002-211753

11. SUPPLEMENTARY NOTES
This work was performed under NASA Langley Research Center research cooperative agreement no. NCC1-01029 entitled, "Development of an Efficient Binaural Simulation for the Analysis of Structural Acoustic Data."
Langley Technical Monitor: Stephen A. Rizzi

12a. DISTRIBUTION/AVAILABILITY STATEMENT
Unclassified-Unlimited
Subject Category 71 Distribution: Standard
Availability: NASA CASI (301) 621-0390

12b. DISTRIBUTION CODE

13. ABSTRACT *(Maximum 200 words)*
Binaural or "virtual acoustic" representation has been proposed as a method of analyzing acoustic and vibro-acoustic data. Unfortunately, this binaural representation can require extensive computer power to apply the Head Related Transfer Functions (HRTFs) to a large number of sources, as with a vibrating structure. This work focuses on reducing the number of real-time computations required in this binaural analysis through the use of Singular Value Decomposition (SVD) and Equivalent Source Reduction (ESR). The SVD method reduces the complexity of the HRTF computations by breaking the HRTFs into dominant singular values (and vectors). The ESR method reduces the number of sources to be analyzed in real-time computation by replacing sources on the scale of a structural wavelength with sources on the scale of an acoustic wavelength. It is shown that the effectiveness of the SVD and ESR methods improves as the complexity of the source increases. In addition, preliminary auralization tests have shown that the results from both the SVD and ESR methods are indistinguishable from the results found with the exhaustive method.

14. SUBJECT TERMS
Binaural simulation, Virtual acoustic simulation, Head related transfer function, Singular value decomposition, Equivalent source reduction

15. NUMBER OF PAGES
44

16. PRICE CODE

17. SECURITY CLASSIFICATION OF REPORT	18. SECURITY CLASSIFICATION OF THIS PAGE	19. SECURITY CLASSIFICATION OF ABSTRACT	20. LIMITATION OF ABSTRACT
Unclassified	Unclassified	Unclassified	UL